Earth and Planetary Science Letters 449 (2016) 240–245

Contents lists available at ScienceDirect

Earth and Planetary Science Letters

www.elsevier.com/locate/epsl

InSAR observations of lake loading at Yangzhuoyong Lake, Tibet: Constraints on crustal elasticity

Wenliang Zhao [a,*], Falk Amelung [a], Marie-Pierre Doin [b], Timothy H Dixon [c], Shimon Wdowinski [a], Guoqing Lin [a]

[a] Department of Marine Geosciences, Rosenstiel School of Marine and Atmospheric Science, University of Miami, 4600 Rickenbacker Causeway, Miami, FL 33149, USA
[b] ISTerre, CNRS, Univ. Joseph Fourier, Grenoble, France
[c] School of Geosciences, University of South Florida, Tampa, FL, USA

ARTICLE INFO

Article history:
Received 29 December 2015
Received in revised form 12 May 2016
Accepted 25 May 2016
Available online 17 June 2016
Editor: B. Buffett

Keywords:
InSAR time-series
surface loading
layered elastic half-space
Young's modulus
crustal elasticity

ABSTRACT

We use Envisat 2003–2010 InSAR imagery over Yangzhuoyong Lake in southeastern Tibet to study the elastic response of the Earth's crust to variations in lake level. The net lake level drop during our study period is ~3 m with seasonal variations of more than 1 m. The time-series close to the lake center shows a high correlation with the lake level history. Near the lake center the unit response with respect to lake level change is 2.5 mm/m in radar line-of-sight direction, or ~2.7 mm/yr in vertical direction, corresponding to a vertical response of ~4.3 mm/Gt load change. We show that the observations are most sensitive to the elastic properties of the crust in the 5–15 km depth range and explain them with a layered elastic half-space model with a Young's modulus of 50 ± 9 GPa Young's modulus in the top 15 km of the crust and using moduli inferred from seismology at greater depth. The inferred Young's modulus is ~25% smaller than the seismic modulus, which we attribute to damaged rock and the presence of fluids.

1. Introduction

Observations of the instantaneous response of the Earth to mass changes along the surface, such as the retreating and growing of ice sheets (Grapenthin et al., 2006; Bevis et al., 2012; Auriac et al., 2014; Zhao et al., 2014), lakes (Bevis et al., 2004; Cavalie et al., 2007; Nof et al., 2012; Wahr et al., 2013; Doin et al., 2015), rivers (Bevis et al., 2005), ocean tide loading (Ito and Simons, 2011) and loading by variations of terrestrial water storage (van Dam et al., 2007; Steckler et al., 2010; Fu and Freymueller, 2012; Chanard et al., 2014) and snow (Heki, 2001), provide an opportunity to better constrain the elastic structure within the Earth's lithosphere and mantle.

Most geodynamic studies infer the elastic structure from seismic wave speed measurements. This is a valid approach at the confining pressures in the lower crust and mantle but not always at the lower pressures in the uppermost crust. In the presence of fluid-filled pores and cracks the moduli depend on strain amplitude and frequency (Fjaer et al., 2008, chapter 5; Adelinet et al., 2010).

The upper crustal elastic moduli are required for the interpretation of surface displacement observations in terms of many geophysical processes including for fault slip distributions of earthquakes and their induced stress changes, the overpressure in volcanic magma reservoirs (e.g. Fukushima et al., 2005; Grapenthin et al., 2010; Grosfils et al., 2013; Heap et al., 2014), and to isolate internal from surface forcings (e.g. Amos et al., 2014; Chamoli et al., 2014; Odbert et al., 2015). The effect of variations of the elastic properties for surface loading problems has been discussed by Dill et al. (2015).

In this study we probe the Young's modulus of the Tibetan crust using InSAR observations of the crustal response to lake loading. The volumes of the lakes on the Tibetan plateau are changing because of the changing climate (Liao et al., 2013). Most lakes are growing because of increased glacier melting and increased precipitation, but some lakes are receding.

2. Background

Yangzhuoyong Lake, also referred to as Yamzho Yumco, is an endorheic lake (Zhang et al., 2013) at 4440 m elevation with a surface area of ~643 km^2 (east–west 130 km, north–south 70 km) an average water depth of 30–40 m (maximum depth of 59 m), draining a ~6100 km^2 basin (Chu et al., 2012a, 2012b). The topography

* Corresponding author.
E-mail address: wenliang.zhao@rsmas.miami.edu (W. Zhao).

http://dx.doi.org/10.1016/j.epsl.2016.05.044
0012-821X/

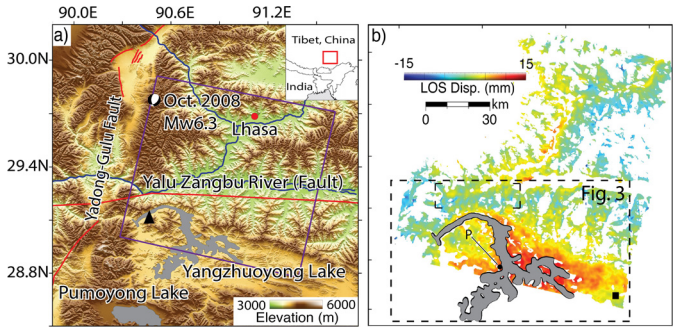

Fig. 1. a) Topographic relief of the study area around Yangzhuoyong Lake. Black triangle: Baidi water level gauge; purple rectangle: SAR coverage (track 405, frame 3015); gray shadings: lakes. b) 2003–2010 InSAR LOS displacement map. Solid square: reference point; dashed rectangle: area of Fig. 3; small rectangle north of lake: area for the estimation of uncertainty of the time-series.

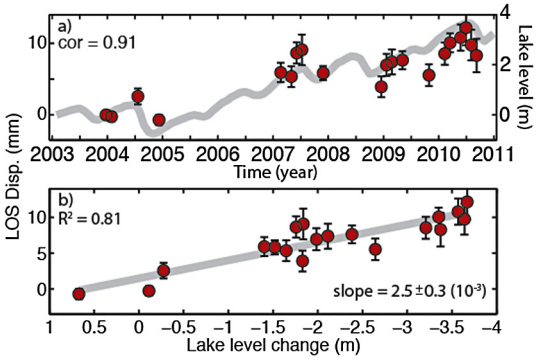

Fig. 2. a) LOS displacement time-series relative to the first acquisition for point P (red dots, see location in Fig. 1b together with the monthly lake level at the Baidi gauge relative to December 2003, the month of the first SAR acquisition (gray line, negative numbers correspond to lake level decrease). Error bars: standard deviation of LOS displacement at each epoch for the non-deforming area northwest of the lake (rectangle in Fig. 1). b) LOS displacement as a function of lake level change (red dots). The slope (gray line) is the LOS displacement with respect to unit lake level change (d^j, unit mm/m). (For interpretation of the references to color in this figure legend, the reader is referred to the web version of this article.)

varies from 3500 m to 5000 m north of the lake to up to 7000 m south of the lake (Fig. 1a). The crustal thickness is about 70 km close to the Yalu Zangbu river, and gradually decreases to 40 km towards the south (Institute of Geology and Geophysics, 1981). The major tectonic structures in the area are the Yalu Zangbu fault zone and Yadong-Gulu rift. A 2008 M_w 6.3 normal faulting earthquake is evidence for active extension across this rift (Sun et al., 2011).

Optical remote sensing shows that Yangzhuoyong Lake retreated by ~80 km^2 between 1970 and 2010 (Li et al., 2014). A lake level gauge (Chu et al., 2012a, 2012b) at Baidi (Fig. 1a) recorded a water level decline of about 5 m since 1970 [see Figure S1 in the supporting information], of which 3 m occurred during the 2003–2010 observation period of this study (gray line in Fig. 2a). The low stands of the lake occur between May and July and the high stands between September and November of each year. Satellite laser altimetry data also show a drop in lake level (Zhang et al., 2011). The lake level decline appears to correlate with increases in air temperature and potential evaporation, suggesting that these are the drivers for lake retreat (Liao et al., 2013).

3. InSAR analysis

Our analysis is based on 27 Envisat ASAR images acquired between December 2003 and September 2010. We discard one SAR acquisition (Nov. 02, 2004) because of strong atmospheric delays. Using spatial and temporal baseline thresholds of 450 m and 4 yr, respectively, we are left with a network of 92 interferograms connecting 20 acquisitions (see Figure S2 in the supporting information).

For data processing we use an approach based on the ROI_PAC software adapted for regions with strong topographic relief (Doin et al., 2011; Grandin et al., 2012). The imagery is coregistered using orbital information and offset fields. The topographic phase is removed using a 3 arc-second SRTM digital elevation model, interpolated to 1 arc-second spacing. Then take 2 looks in range and 10 looks in azimuth direction to obtain ~40 × 40 m^2 ground pixel. Next, we remove contributions from topography-correlated tropospheric delays and localized DEM errors from the wrapped interferograms to aid phase-unwrapping. The first is estimated using a second-order polynomial with respect to elevation (Cavalie et al., 2007; Nof et al., 2012, see Figure S3a, b in the supporting information for an example). The second is estimated from a set of interferograms using the method of Ducret et al. (2014) (see Figure S3c, d in the supporting information). For this processing step we use all available SAR acquisitions, including interferograms with baselines larger than 450 m. Next, we take additional looks to obtain ~80 × 80 m^2 pixels, apply an adaptive filter, and unwrap the phase. We retain only pixels with a spatial coherence larger than 0.2 in 60 percent of the interferograms (e.g. Baker and Amelung, 2012). We reduce phase unwrapping errors of isolated areas using the nearest-neighbor interpolation method of Shanker and Zebker (2009). We then add the tropospheric phase contributions back to the unwrapped phase. This approach of temporarily removing topography-correlated phase contributions, combined with the localized DEM correction, improves the phase unwrapping because it reduces the spatial standard deviation of the wrapped phase, ensuring that multi-looking and filtering increases the SNR without blurring the signal.

We then use the small baselines (SB) InSAR time-series approach to obtain pixel wise displacement histories (Berardino et al., 2002). Finally, in the time domain we remove the topography-correlated phase due to tropospheric layering from the unwrapped phase using a second-order polynomial, and correct for topographic residuals using the approach of Fattahi and Amelung (2013). We validated the results using atmospheric corrections based on MERIS observations and the ERA-Interim atmospheric model (see Figure S7 in the supporting information).

4. Results

The ground displacement field in radar line-of-sight (LOS) direction shows a bulge of up to 9 mm LOS displacement near the lake (red colors, Fig. 1b), corresponding to ~10 mm of uplift assuming that displacement is vertical (with a radar incidence angle on the ground of ~23° Envisat's I2 beam is most sensitive to vertical deformation). To the north of the lake where the topographic relief is up to 2500 m, LOS variations likely represent residual tropospheric delays.

A displacement time series for a point near the lake center (Fig. 2a) shows the correlation between ground displacement and lake level (gray line) (Fig. 2a). Seasonal drops in lake level (negative lake level changes) coincide with LOS decreases (uplift) and seasonal rises in lake level (positive lake level changes) coincide with LOS increases (subsidence). The correlation between the sign-reversed lake level and displacement is 0.9.

The LOS displacement u_i^j, at pixel j and epoch i, relates to the lake level, l_i, by $u_i^j = d^j \times l_i$ with d^j the LOS displacement with respect to unit lake level change or unit response of the system at pixel j (in mm/m or 10^{-3}). Both u_i^j and l_i are relative to the first SAR acquisition. The least squares solution for d^j is given by

$$\left[d^j\ c^j\right] = \left(\mathbf{G}^T\mathbf{G}\right)^{-1}\mathbf{G}^T\mathbf{u}^j \quad (1)$$

with $\mathbf{u}^j = (u_1^j, u_2^j, \ldots, u_N^j)^T$, c^j the constant for least square fitting, and $\mathbf{G} = [(l_1, l_2, \ldots, l_N)^T, (1, 1, \ldots, 1)^T]$. An example for d^j at point P is given in Fig. 2b. The maximum LOS displacement with respect to unit lake level change is 2.5 mm/m close to the lake center, corresponding to 2.7 mm/yr vertical displacement.

5. Modeling

We use layered elastic half-space models (Cavalie et al., 2007) to simulate the observed rebound in LOS direction and geophysical inverse methods to estimate Young's modulus in the crust. We use a Poisson's ratio of 0.25 as it cannot be constrained by the dominantly vertical displacements in response to surface loading because of the trade-off with Young's modulus (see Green's functions e.g. in Zhao et al., 2014).

Our data are the LOS displacements with respect to unit lake level change (unit mm/m, see Fig. 2b), calculated for each pixel from the LOS displacement history (Fig. 3a). We use a quadtree decomposition (Sudhaus and Jonsson, 2009) to downsample the data with quadrants selected according to the expected signal (using the layered model with Young's modulus of 40 GPa, quadrant size 1.44 km to 11.52 km, threshold for subdividing of 0.08 mm/m, 315 data blocks; half and doubled Young's modulus give nearly identical sampling). We found that this sampling provided reasonable sensitivity to model variations in both the near and far fields. To find the best-fitting models we minimize the root mean square error (RMSE), defined as:

$$RMSE = \sqrt{(d-p)^T \Sigma^{-1} (d-p)/M} \qquad (2)$$

where $\mathbf{d}$ is the observed and $\mathbf{p}$ the modeled LOS displacement per unit lake level change. $\mathbf{d}$ and $\mathbf{p}$ are $M \times 1$ vectors with M being the number of data blocks after quad-tree decomposition, and $\mathbf{\Sigma}$ is the $M \times M$ variance–covariance matrix used as a weighting matrix, calculated from the sample semi-variogram and covariogram (Sudhaus and Jonsson, 2009) (see Figure S4 in the supporting information for the data weights).

We estimate Young's modulus for the top layer (from the surface to 15 km depth) using a grid search varying the modulus between 30 GPa and 150 GPa at 5 GPa steps. At depth larger than 15 km we use the elastic parameters from seismic wave speed measurements 300 km further north of Yin et al. (1990) and Mechie et al. (2004) instead of a global model (Fig. 4a, b, see Supplementary Material Table S1 in the supporting information); the latter are from 300 km further north. The best fit is found for a modulus of 50 ± 9 GPa in the top layer (Fig. 3) with the standard error obtained from 1000 bootstrap samplings. The RMSE is 0.57 mm/m. The model predictions agree with the observations west and south of the lake but are lower than observed northeast of the lake (Fig. 4c). A model with the seismic moduli (56 GPa from 0–5 km and 71 GPa from 5–15 km, Supplementary Material Table S1) under-predicts the uplift at the center of the lake (see Figure S5a, c in the supplementary material). A west–east profile across the lake (AA′ in Fig. 4) shows that the best-fitting model is associated with higher displacement gradients than the seismic model because of the lower Young's modulus in the top layer.

For completeness we also employed a halfspace model and found a Young's modulus of 81 ± 12 GPa by linear inversion (see Figure S5b in the supporting information).

6. Discussion

InSAR recorded up to ~9 mm ground displacement towards the radar in the vicinity of Yangzhuoyong Lake during 2003–2010. The lake level dropped by more than 3 m during this time period, suggesting that we see rebound caused by the partial removal of the water load. Near the lake center, the response obtained from linear regression is 2.5 mm/m LOS displacements with respect to unit lake level change.

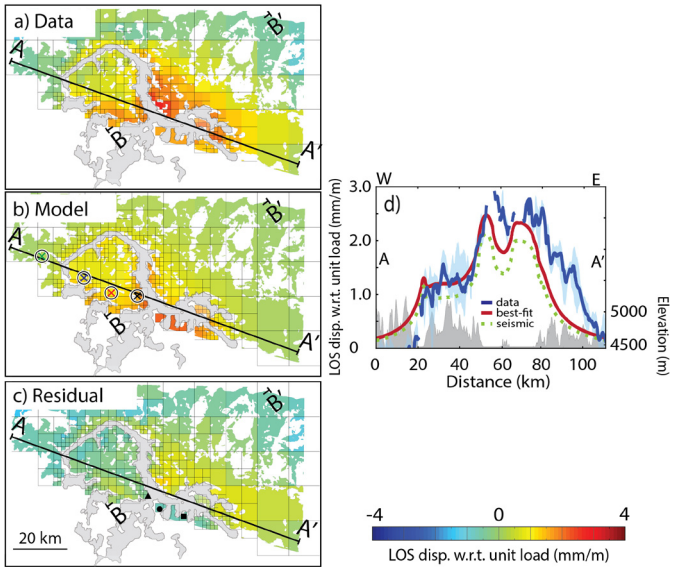

Fig. 3. a) Observed LOS displacement with respect to unit load, b) prediction from the best-fitting layered model (top layer Young's modulus of 50 GPa), c) differences between observations and model predictions, d) profile along AA′ averaged over a width of 1.8 km (dark blue; light blue shows the upper and lower bounds; together with the predictions from the best-fitting model (red line) and the seismic model (dashed green line). Gray shading: topographic elevation along the profile. For profile BB′ see Figure S6 in the supporting information. The colored crosses in b) show the points of Fig. 4. The triangle, circle and square in c) denote the geometric mass center of the load at current lake level and for 100 and 200 m higher lake level, respectively.

6.1. Depth sensitivity

To constrain the depth range of the crust sampled by the lake load we conduct a depth sensitivity test following Doin et al. (2015). We divide the crust into a series of 5 km thick sublayers. Starting from the preferred model we reduce the Young's modulus in each sub-layer by a factor of 2 and compare the surface displacement with that from the preferred model as a function of distance from the load's gravity center. Fig. 4c shows that the reduction in the elasticity parameters in the 5–10 km and 10–15 km sublayers causes the largest increases in surface displacement (0.1–0.3 mm/m at 6–24 km distance with the largest increase of more than 0.3 mm/m at 6 km distance). Changes in the elasticity parameters in the sublayers below 40 km depth have little effect (<0.07 mm/m). This shows that in most parts of the study area the surface response is most sensitive to the 5–15 km depth range. This validates our approach of considering a 15 km-thick top layer.

6.2. Assumptions

We have considered a perfectly elastic model, neglecting possible viscous effects due to load changes prior to the period of our study, which can be important in lake loading studies (e.g. Cavalie et al., 2007; Doin et al., 2015). Several seismic studies have resolved a high conductivity zone in the Tibetan crust (Brown et al., 1996; Nelson et al., 1996). Brown et al. (1996) interpret it is due to partial melt, and Ryder et al. (2007) and Doin et al. (2015) further use it as the evidence of low viscosity in the middle crust. At Yangzhuoyong Lake the current period of lake level drop started only in late 2004. Before that, the lake level first dropped by ~4 m (between 1980 and 1996) and then rose by ~3 m (Figure S1). This

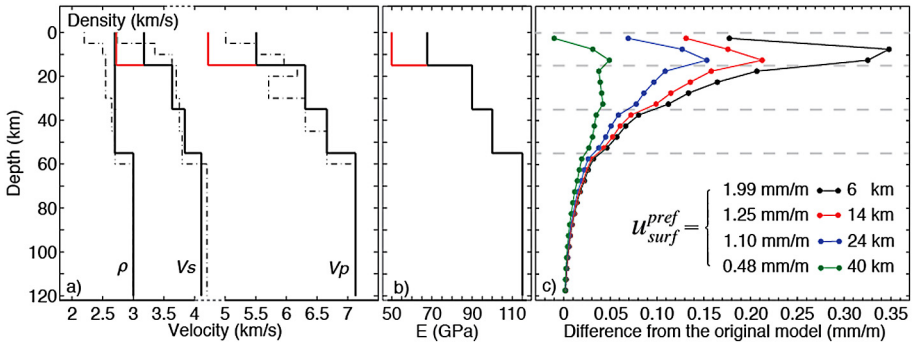

Fig. 4. a) V_P (Yin et al., 1990), V_S and density (Mechie et al., 2004) as a function of depth (dashed lines) together with layer averages (solid lines) and b) corresponding Young's moduli. Red line indicates the Young's modulus of best-fitting model. See Supplementary Material Table S1 in the supplementary material for the numerical values. c) Depth sensitivity test. The colored lines show the difference in surface displacement from the preferred model for four locations at increasing distance from the lake center (see crosses on Fig. 3b, distances in lower right). Each dot represents the center depth of the sub-layer with reduced modulus. u_{surf}^{pref} is the surface LOS displacement of the preferred model at the four locations.

suggests that the viscous effects from these two periods largely compensate each other, justifying the elastic treatment.

We did not consider any changes in underground water content co-occurring with lake level changes because this additional load is small and because the effect on surface deformation would be partly compensated for by poro-elastic deformation.

6.3. Data fit

Our best-fitting models underpredict the displacement response in the area northeast of the lake by 0.5–1 mm/m. We offer two possible explanations for this discrepancy. In one explanation this area is rebounding because of the visco-elastic response from past unloading (the lake level history before 1970 has not been documented). Given the topographic relief, for a 100 and 200 m higher lake level the lake's past center of gravity would be located 12–20 km to the east of the current center of gravity (Fig. 3c). Another explanation is that the upper crust in this area is weaker resulting in more rebound. Seismic reflection studies identified relatively low shallow wave speed velocities (5.2 km/s) (Yin et al., 1990) and partial melt in the middle crust (at 25 km depth) in this area (Brown et al., 1996) but the three-dimensional structure has not been resolved.

6.4. Tropospheric delays

We used a data analysis approach that included the empirical estimation and removal of the topography-correlated phase assuming the phase was caused by atmospheric delays, which could lead to a bias. We also analyzed the data using (i) the cloud free acquisitions and atmospheric delay correction with the MEdium Resolution Imaging Spectrometer (MERIS) observation (Li et al., 2006) and (ii) all acquisitions with atmospheric corrections using the ERA-Interim global atmospheric model (Jolivet et al., 2014). The LOS displacement fields are more noisy but both cases show a signal in the vicinity of the lake (see Figure S7 in the supporting information), making us confident that the signal represents real deformation.

6.5. Comparison with other surface loading problems

For comparison with other loading problems it is useful to express ground displacement in response to mass change. The response next to the lake center corresponds to ~4.3 mm/Gt of load change (for a surface area of 621 km^2, 1.61 m of level change corresponds to 1 Gt mass change). Wahr et al. (2013) reported GPS displacements due to 10 m lake level decrease of Lake Shasta in California (surface area of 120 km^2), corresponding to a response of ~4 mm/Gt, very similar to our observations. However, Bevis et al. (2004) reported a response of 7.4 mm/Gt for the smaller Lago Laja in Chile (surface area 95 km^2). Variations in the magnitude of the response reflect variations in the elastic properties of the rocks, in the load size, and in the distance to the load's center.

6.6. Comparison with seismic moduli

We have found a Young's modulus of 50 ± 9 GPa for the upper crust, given a Poisson's ratio of 0.25 (see Supplementary Material Table S1). The Young's modulus is ~25% lower than the averaged modulus of the regional seismic model of 68 GPa (see Supplementary Material Table S1). A Young's modulus smaller than the seismic modulus is consistent with laboratory measurements which in undrained conditions yield smaller static than dynamic moduli. The static moduli are inferred from stress–strain curves (e.g. Mashinsky, 2003), whereas the dynamic moduli are obtained from seismic and acoustic velocities and from density measurements (Vidal et al., 2002; Adelinet et al., 2010). In contrast, in dry conditions the moduli don't show frequency dispersion (Ciccotti and Mulargia, 2004).

Most studies consider moduli lower than the seismic moduli just in the uppermost crust (Wauthier et al., 2012; Doin et al., 2015). Our investigation suggests that fluid-filled cracks can affect Young's modulus to a depth of ~15 km. Lower-than-expected elastic stiffness was also found for Lago Laja (Bevis et al., 2004).

7. Conclusion

We have documented a total of 9 mm of ground surface displacement towards the satellite in the vicinity of Yangzhuoyong Lake between 2003 and 2010. We attribute this signal to crustal rebound due to lake level changes of more than ~3 m during this time period. Assuming that underground water content changes do not contribute to the load, we explain the signal as the elastic response of a layered half-space with a Young's modulus of 50 ± 9 GPa in the top layer (thickness of 15 km), which is ~25% less than the seismic modulus. The lake load is most sensitive to the elastic properties at 5–15 km depth range, suggesting that fluid-filled cracks in this depth range can affect Young's modulus.

Acknowledgements

We thank Duo Chu for providing lake level records. We also thank two anonymous reviewers for their helpful comments. This study was supported by a grant from NASA's cryospheric program to F.A. (Grant No. NNX13AP95G).

Appendix A. Supplementary material

Supplementary material related to this article can be found online at http://dx.doi.org/10.1016/j.epsl.2016.05.044.

References

Adelinet, M., Fortin, J., Gueguen, Y., Schubnel, A., Geoffroy, L., 2010. Frequency and fluid effects on elastic properties of basalt: experimental investigations. Geophys. Res. Lett. 37 (2). http://dx.doi.org/10.1029/2009GL041660.

Amos, C.B., Audet, P., Hammond, W.C., Burgmann, R., Johanson, I.A., Blewitt, G., 2014. Uplift and seismicity driven by groundwater depletion in central California. Nature 509, 483–486. http://dx.doi.org/10.1038/nature13275.

Auriac, A., Sigmundsson, F., Hooper, A., Spaans, K.H., Bjornsson, H., Palsson, F., Pinel, V., Feigl, K.L., 2014. InSAR observations and models of crustal deformation due to a glacial surge in Iceland. Geophys. J. Int. 198 (3), 1329–1341. http://dx.doi.org/10.1093/gji/ggu205.

Baker, S., Amelung, F., 2012. Top-down inflation and deflation at the summit of Kīlauea Volcano, Hawaii observed with InSAR. J. Geophys. Res. http://dx.doi.org/10.1029/2011JB009123.

Berardino, P., Fornaro, G., Lanari, R., Sansosti, E., 2002. A new algorithm for surface deformation monitoring based on small baseline differential SAR interferograms. IEEE Trans. Geosci. Remote Sens. 40, 2375–2383. http://dx.doi.org/10.1109/TGRS.2002.803792.

Bevis, M., Kendrick, E., Cser, A., Smalley Jr., R., 2004. Geodetic measurement of the local elastic response to the changing mass of water in Lago Laja, Chile. Phys. Earth Planet. Inter. 141, 71–78. http://dx.doi.org/10.1016/j.pepi.2003.05.001.

Bevis, M., Alsdorf, D., Kendrick, E., Fortes, L.P., Forsberg, B., Smalley Jr., R., Becker, J., 2005. Seasonal fluctuations in the mass of the Amazon River system and Earth's elastic response. Geophys. Res. Lett. 32, L16308. http://dx.doi.org/10.1029/2005GL023491.

Bevis, M., et al., 2012. Bedrock displacements in Greenland manifest ice mass variations, climate cycles and climate change. Proc. Natl. Acad. Sci. USA 109 (30), 11944–11948.

Brown, L.D., Zhao, W., Nelson, K.D., Hauck, M., Alsdorf, D., Ross, A., Cogan, M., Clark, M., Liu, X., Che, J., 1996. Bright spots, structure, and magmatism in southern Tibet from INDEPTH seismic reflection profiling. Science 274 (5293), 1688–1690. http://dx.doi.org/10.1126/science.274.5293.1688.

Cavalie, O., Doin, M.-P., Lasserre, C., Briole, P., 2007. Ground motion measurement in the Lake Mead area, Nevada, by differential synthetic aperture radar interferometry time series analysis: probing the lithosphere rheological structure. J. Geophys. Res. 112, B03403. http://dx.doi.org/10.1029/2006JB004344.

Chamoli, A., Lowry, A.R., Jeppson, T.N., 2014. Implications of transient deformation in the northern Basin and Range, western United States. J. Geophys. Res. 119 (5), 4393–4413. http://dx.doi.org/10.1002/2013JB010605.

Chanard, K., Avouac, J.P., Ramillien, G., Genrich, J., 2014. Modeling deformation induced by seasonal variations of continental water in the Himalaya region: sensitivity to Earth elastic structure. J. Geophys. Res. http://dx.doi.org/10.1002/2013JB010451.

Chu, D., Wang, D., Pu, Q., De, J., La, B., Pu, B., Zhang, X., Sun, R., 2012a. A model for the remote sensing monitoring of Yangzhuoyong lake and recent variation. Chin. J. Glaciol. Geocryol. 34 (3). http://dx.doi.org/1000-0240(2012)03-0530-08 (in Chinese).

Chu, D., Qiong, P., Wang, D., Mima, C., Laba, Z., Zhang, X., Sun, R., 2012b. Water level variations of Yamzho Yumco Lake in Tibet and the main driving forces. J. Mt. Sci. 30 (2). http://dx.doi.org/1008-2786-(2012)2-239-09 (in Chinese).

Ciccotti, M., Mulargia, F., 2004. Differences between static and dynamic elastic moduli of a typical seismogenic rock. Geophys. J. Int. 157, 474–477. http://dx.doi.org/10.1111/j.1365-246X.2004.02213.x.

van Dam, T., Wahr, J., Lavallée, D., 2007. A comparison of annual vertical crustal displacements from GPS and Gravity Recovery and Climate Experiment (GRACE) over Europe. J. Geophys. Res., Solid Earth (1978–2012) 112 (B3). http://dx.doi.org/10.1029/2006JB004335.

Dill, R., Klemann, V., Martinec, Z., Tesauro, M., 2015. Applying local Green's functions to study the influence of the crustal structure on hydrological loading displacements. J. Geodyn. 88, 14–22. http://dx.doi.org/10.1016/j.jog.2015.04.005.

Doin, M.P., Lodge, F., Guillaso, S., Jolivet, R., Lasserre, C., Ducret, G., Grandin, R., Pathier, E., Pinel, V., 2011. Presentation of the small baseline NSBAS processing chain on a case example: the Etna deformation monitoring from 2003 to 2010 using Envisat data. In: Proc. ESA Fringe, vol. 2011.

Doin, M.P., Twardzik, C., Ducret, G., Lasserre, C., Guillaso, S., Jianbao, S., 2015. InSAR measurement of the deformation around Siling Co Lake: inferences on the lower crust viscosity in central Tibet. J. Geophys. Res., Solid Earth. http://dx.doi.org/10.1002/2014JB011768.

Ducret, G., Doin, M.P., Grandin, R., Lasserre, C., Guillaso, S., 2014. DEM corrections before unwrapping in a small baseline strategy for InSAR time series analysis. IEEE Geosci. Remote Sens. Lett. 11 (3). http://dx.doi.org/10.1109/LGRS.2013.2276040.

Fattahi, H., Amelung, F., 2013. DEM error correction in InSAR time series. IEEE Trans. Geosci. Remote Sens. 51 (7), 4249–4259. http://dx.doi.org/10.1109/TGRS.2012.2227761.

Fjaer, E., Holt, R.M., Horsrud, P., Raaen, A.M., Risnes, R., 2008. Petroleum Related Rock Mechanics, 2nd edition. Elsevier.

Fu, Y., Freymueller, J.T., 2012. Seasonal and long-term vertical deformation in Nepal Himalaya constrained by GPS and GRACE measurements. J. Geophys. Res. 117, B03407. http://dx.doi.org/10.1029/2011JB008925.

Fukushima, Y., Cayol, V., Durand, P., 2005. Finding realistic dike models from interferometric synthetic aperture radar data: the February 2000 eruption at Piton de la Fournaise. J. Geophys. Res. 110 (B3). http://dx.doi.org/10.1029/2004JB003268.

Grandin, R., Doin, M-P., Bollinger, L., Pinel-Puyssegur, B., Ducret, G., Jolivet, R., Sapkota, S.N., 2012. Long-term growth of the Himalaya inferred from interseismic InSAR measurement. Geology 40 (12), 1059–1062. http://dx.doi.org/10.1130/G33154.1.

Grapenthin, R., Sigmundsson, F., Geirsson, H., Árnadóttir, T., Pinel, V., 2006. Icelandic rhythmics: annual modulation of land elevation and plate spreading by snow load. Geophys. Res. Lett. 33, L24305. http://dx.doi.org/10.1029/2006GL028081.

Grapenthin, R., Ófeigsson, B.G., Sigmundsson, F., Sturkell, E., Hooper, A., 2010. Pressure sources versus surface loads: analyzing volcano deformation signal composition with an application to Hekla volcano, Iceland. Geophys. Res. Lett. 37 (20). http://dx.doi.org/10.1029/2010GL044590.

Grosfils, E.B., McGovern, P.J., Gregg, P.M., Galgana, G.A., Hurwitz, D.M., Long, S., Chestler, S., 2013. Elastic models of magma reservoir mechanics: a key tool for understanding planetary volcanism. In: Massironi, M., et al. (Eds.), Volcanism and Tectonism Across the Solar System. In: Geol. Soc. London Spec. Publ. SP401.

Heap, M.J., Baud, P., Meredith, P.G., Vinciguerra, S., Reuschlé, T., 2014. The permeability and elastic moduli of tuff from Campi Flegrei, Italy: implications for ground deformation modelling. Solid Earth 5 (1), 25–44.

Heki, K., 2001. Seasonal modulation of interseismic strain buildup in northeastern Japan driven by snow loads. Science 293 (5527), 89–92. http://dx.doi.org/10.1126/science.1061056.

Institute of Geology and Geophysics, Chinese Academy of Sciences, 1981. Explosion seismic study for velocity distribution and structure of the crust and upper mantle from Damxung to Yadong of Xizang plateau. Acta Geophys. Sin. 24 (2), 156–170.

Ito, T., Simons, M., 2011. Probing asthenospheric density, temperature, and elastic moduli below the western United States. Science 332 (6032), 947–951. http://dx.doi.org/10.1126/science.1202584.

Jolivet, R., Agram, P.S., Lin, N.Y., Simons, M., Doin, M.-P., Peltzer, G., Li, Z., 2014. Improving InSAR geodesy using global atmospheric models. J. Geophys. Res. 119 (3), 2324–2341. http://dx.doi.org/10.1002/2013JB010588.

Li, L., Li, J., Yao, X., Luo, J., Huang, Y., Feng, Y., 2014. Changes of the three holy lakes in recent years and quantitative analysis of the influencing factors. Quat. Int., 1–7. http://dx.doi.org/10.1016/j.quaint.2014.04.051.

Li, Z., Fielding, E.J., Cross, P., Muller, J.-P., 2006. Interferometric synthetic aperture radar atmospheric correction: medium resolution imaging spectrometer and advanced synthetic aperture radar integration. Geophys. Res. Lett. 33 (6). http://dx.doi.org/10.1029/2005GL025299.

Liao, J., Shen, G., Li, Y., 2013. Lake variations in response to climate change in the Tibetan Plateau in the past 40 years. Int. J. Digit. Earth 6 (6), 534–549. http://dx.doi.org/10.1080/17538947.2012.656290.

Mashinsky, E.I., 2003. Differences between static and dynamic elastic moduli of rocks: physical causes. Russ. Geol. 44 (9), 953–959.

Mechie, J., Sobolev, S.V., Ratschbacher, L., Bock, G., Jones, A.G., Nelson, K.D., Brown, L.D., Zhao, W., 2004. Precise temperature estimation in the Tibetan crust from seismic detection of the $\alpha - \beta$ quartz transition. Geology 32 (7), 601–604. http://dx.doi.org/10.1130/G20367.1.

Nelson, K.D., et al., 1996. Partially molten middle crust beneath southern Tibet: synthesis of project INDEPTH results. Science 274 (5293), 1684–1688.

Nof, R.N., Ziv, A., Doin, M.-P., Baer, G., Fialko, Y., Wdowinski, S., Eyal, Y., Bock, Y., 2012. Rising of the lowest place on Earth due to Dead Sea water-level drop: evidence from SAR interferometry and GPS. J. Geophys. Res. 117, B05412. http://dx.doi.org/10.1029/2011JB008961.

Odbert, H., Taisne, B., Gottsmann, J., 2015. Deposit loading and its effect on co-eruptive volcano deformation. Earth Planet. Sci. Lett. 413, 186–196. http://dx.doi.org/10.1016/j.epsl.2015.01.005.

Ryder, I., Parsons, B., Wright, T.J., Funning, G.J., 2007. Post-seismic motion following the 1997 Manyi (Tibet) earthquake: InSAR observations and modeling. Geophys. J. Int. 169, 1009–2027. http://dx.doi.org/10.1111/j.1365-246X.2006.03312.x.

Shanker, P., Zebker, H., 2009. Sparse two dimensional phase unwrapping using regular grid methods. IEEE Geosci. Remote Sens. Lett. 6 (2), 327–331.

Steckler, M.S., Nooner, S.L., Akhter, S.H., Chowdhury, S.K., Bettadpur, S., Seeber, L., Kogan, M.G., 2010. Modeling Earth deformation from monsoon flooding in Bangladesh using hydrographic, GPS, and Gravity Recovery and Climate Experiment (GRACE) data. J. Geophys. Res. 115, B08407. http://dx.doi.org/10.1029/2009JB007018.

Sudhaus, H., Jonsson, S., 2009. Improved source modelling through combined use of InSAR and GPS under consideration of correlated data errors: application to the June 2000 Kleifarvatn earthquake, Iceland. Geophys. J. Int. 176, 389–404. http://dx.doi.org/10.1111/j.1365-246X.2008.03989.x.

Sun, J., Johnson, K.M., Cao, Z., Shen, Z., Burgmann, R., Xu, X., 2011. Mechanical constraints on inversion of coseismic geodetic data for fault slip and geometry: example from InSAR observation of the 6 October 2008 M_w 6.3 Dangxiong–Yangyi (Tibet) earthquake. J. Geophys. Res. 116, B01406. http://dx.doi.org/10.1029/2010JB007849.

Vidal, S., Longuemare, P., Huguet, F., Mechler, P., 2002. Reservoir parameters quantification from seismic monitoring integrating geomechanics. Oil Gas Sci. Technol. 57 (5), 555–568. http://dx.doi.org/10.2516/ogst:2002037.

Wahr, J., Khan, S.A., van Dam, T., Liu, L., van Angelen, J.H., van den Broeke, M.R., Meertens, C.M., 2013. The use of GPS horizontals for loading studies, with applications to northern California and southeast Greenland. J. Geophys. Res. 118 (4), 1795–1806. http://dx.doi.org/10.1002/jgrb.50104.

Wauthier, C., Cayol, V., Kervyn, F., d'Oreye, N., 2012. Magma sources involved in the 2002 Nyiragongo eruption, as inferred from an InSAR analysis. J. Geophys. Res. 177 (B5). http://dx.doi.org/10.1029/2011JB008257.

Yin, Z., Teng, J., Liu, H., 1990. The 2-D crustal structure study in the Yadong-Damxung region of the Xizang plateau. Bull. Chin. Acad. Geol. Sci. 21, 239–244 (in Chinese).

Zhang, G., Xie, H., Kang, S., Yi, D., Ackley, S.F., 2011. Monitoring lake level changes on the Tibetan plateau using ICESat altimetry data (2003–2009). Remote Sens. Environ. 115, 1733–1742. http://dx.doi.org/10.1016/j.rse.2011.03.005.

Zhang, G., Yao, T., Xie, H., Kang, S., Lei, Y., 2013. Increased mass over the Tibetan Plateau: from lakes or glaciers? Geophys. Res. Lett. 40 (10), 2125–2130. http://dx.doi.org/10.1002/grl.50462.

Zhao, W., Amelung, F., Dixon, T.H., Wdowinski, S., Malservisi, R., 2014. A method for estimating ice loss from relative InSAR observations: application to the Vatnajökull ice cap, Iceland. Geochem. Geophys. Geosyst. 15 (1), 108–120. http://dx.doi.org/10.1002/2013GC004936.